analytical chemistry

Feature

pubs.acs.org/ac

Mass Spectrometry Imaging of Therapeutics from Animal Models to Three-Dimensional Cell Cultures

Mass spectrometry imaging (MSI) is a powerful label-free technique for the investigation of the spatial distribution of molecules at complex surfaces and has been widely used in the pharmaceutical sciences to understand the distribution of different drugs and their metabolites in various biological samples, ranging from cell-based models to tissues. Here, we review the current applications of MSI for drug studies in animal models, followed by a discussion of the novel advances of MSI in three-dimensional (3D) cell cultures for accurate, efficient, and high-throughput analyses to evaluate therapeutics.

Xin Liu and Amanda B. Hummon*

Department of Chemistry and Biochemistry, Harper Cancer Research Institute, University of Notre Dame, 251 Nieuwland Science Hall, Notre Dame, Indiana 46556, United States

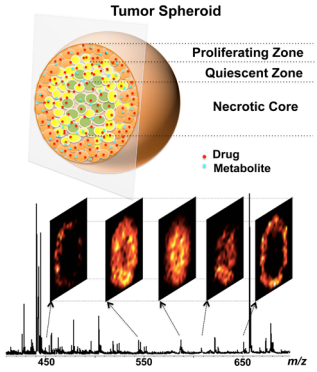

In the process of searching for new medicines to improve the quality of human life, detailed understanding of a drug's absorption, distribution, metabolism, and excretion (ADME) has fundamental significance in determining the efficacy or toxicological properties of the pharmaceutical substance. To understand a drug's distribution, imaging approaches are needed. Autoradiography,[1] positron emission tomography (PET),[2] magnetic resonance imaging (MRI),[3] and fluorescence imaging[4] are commonly used approaches to examine the spatial distribution of a drug in laboratory animals. These traditional imaging methods require radioisotopes and magnetic or imaging probes.

In autoradiography methods, a radiolabel is attached to the pharmaceutical of interest prior to dosing. In the experiment, the radiolabel is imaged, not the compound itself. Thus, one intrinsic limitation of this technology is the inability to distinguish the localization of a parent drug and its potential metabolites. There are two types of radiography commonly used to image drugs and their metabolites. Macroautoradiography (MARG) is a histological technique that entails a detailed spatial imaging of radioactivity in tissues at the cellular level (typical spatial resolution of 10 μm).[5] In contrast, whole body autoradiography (WBA), with typical spatial resolutions of 100 μm, has the ability to show the distribution of radiolabeled substances in all organs of an intact animal carcass.[4] Due to its more limited spatial resolution, WBA is often combined with liquid chromatography mass spectrometry (LC-MS),[6] which is capable of identification and quantification of the compound and metabolites from tissue extracts, to gain specific distribution information.

Both PET and MRI require the use of labels. Radioactive isotope labels are used in the PET technique. For MRI analysis, drugs typically need to contain ^{19}F or be enriched in ^{13}C to be visualized in vivo as the sensitivity depends on the magnetic properties of the monitored nucleus.[7] Though PET and MRI can be employed to perform drug-imaging studies, they suffer from millimeter spatial resolution as well as low specificity and limited molecular information. Other labeled imaging techniques, such as fluorescent microscopy, require a drug molecule to be modified with a chemical tag, which can affect its pharmacological properties, drug uptake, and localization within the body.

Mass spectrometry imaging (MSI) is an interesting alternative used in a growing number of ADME studies and pharmaceutical compound investigations. Many excellent MSI reviews describing drug studies have been published in recent years.[8−14] MSI possesses nanometer scale spatial resolution. It provides the chemical specificity of mass spectrometry to allow direct mapping of a parent drug or prodrug without any labeling. MSI also enables simultaneous detection of the active and toxic metabolites of a pharmaceutical compound to gain a better understanding of the efficacy and toxicity properties of the drug.

Briefly, in MSI experiments, sectioned biological specimens are placed in a mass spectrometer and an ordered array of mass spectra are acquired from a raster of positions across the sample surface. Ion density maps can then be reconstructed for any selected peak of a particular mass from the data set in which each pixel consists of a mass spectrum or multiple MS/MS transitions. Various mass spectrometry ionization techniques have been developed for MSI in biological samples. Due to space limitations, a few ionization techniques will be discussed, but only matrix-assisted laser desorption/ionization (MALDI) will be described in detail below. The novel application of MALDI-MSI in three-dimensional (3D) cell cultures as a platform for drug evaluation will then be introduced.

Published: June 18, 2015

DOI: 10.1021/acs.analchem.5b00419
Anal. Chem. 2015, 87, 9508−9519

MALDI AND ITS APPLICATIONS

MALDI is one of the most widely employed ionization techniques used to visualize the spatial arrangement of drugs and metabolites in tissue.[15−19] In a typical MALDI-MSI experiment, a UV-absorbing matrix is carefully applied on the surface of a tissue section to assist desorption and ionization of analytes in the sample. Following irradiation by a laser beam in an array of discrete points, mass spectra are generated for each *x*, *y* coordinate and images of interest are generated.

Troendel et al. first used MALDI-MSI for direct profiling of the drug paclitaxel in tissues in 1999.[20] In 2003, the first MS images of drug distribution in a rat brain were reported by the Caprioli group.[21] Various pharmaceutical compounds such as clozapine,[22] erlotinib,[23] olanzapine,[24,25] oxaliplatin,[26] and terfenadine[27] have subsequently been investigated, and their metabolites have been imaged in different tissue sections and cells. Figure 1a shows whole-body MSI images generated with a hybrid MALDI-LTQ-Orbitrap-MS to detect the distribution of reserpine and its metabolites at 2 h following a 20 mg/kg oral dose.[28] The results show that reserpine was found to mostly localize in the stomach and testis of the rat. In addition, the accumulation of the known reserpine metabolites methyl reserpate and reserpic acid in the intestines, muscle, thoracic cavity, and liver indicates extensive metabolism of reserpine. The simultaneous imaging of both the drug and the resulting metabolites shows a significant advantage of MALDI-MSI over conventional WBA.

There have been great advances in the use of MALDI-MSI in recent years to expand its applications, and here, we review some methodological developments that can be helpful for successful drug evaluation, including improvements in sample preparation, instrumentation, data acquisition, and analysis.

CRYOSECTIONING AND WASHING

After harvesting biological samples for MALDI-MSI, they are snap frozen and stored at −80 °C until sliced into thin sections ranging from 3 to 50 μm with a cryostat.[11] The thickness of the sample can be a significant factor, which influences the spectrum quality, such as the signal-to-noise ratio, especially for molecules present at low concentrations. Tissue slices thicker than 20 μm can result in a degraded spectrum, which also affect the quality of imaging results.[29] Thus, thickness of tissue slices needs to be optimized for best detection efficiency and spectral quality. The sections are then thaw-mounted onto a MALDI stainless steel plate, electrically conductive or nonconductive glass slide depending on the sample preparation requirements of the specific MALDI mass spectrometer.

For the evaluation of therapeutics, washing the slides is not advised to avoid delocalization or substantial/total loss of the drug compounds in organic solvents. However, a pH-controlled tissue washing protocol recently developed for MALDI-MSI has been shown to help improve the limits of detection for low-molecular weight compounds, like the drug cimetidine, imipramine, and a protease inhibitor compound C, in sections.[30] This protocol involves washing the slides with a buffer solution. This buffer solution is pH adjusted so that the target molecules have low solubility in order to remove suppressant species from the tissue and improve the signal-to-noise ratio without significant delocalization of the analytes of interest during the cleanup procedure. As a result, the signal-to-noise ratio was increased by a factor of 10. This protocol can be beneficial for researchers in pharmaceutical fields using MALDI-MSI.

MATRIX SELECTION AND APPLICATION

Before performing MALDI-MSI, the choice and application of matrix is significant to obtain high quality imaging results and should be optimized for each type of experiment. Small molecule (<700 Da) analysis is sometimes challenging due to the background noise of organic matrices, which can suppress or overlap with the *m*/*z* of the analytes. For this reason, different matrices should be tested when investigating a specific small compound in order to select the one that provides the greatest selectivity and sensitivity by promoting ionization of the analytes of interest without increasing the background ions. The most commonly used matrices in drug and metabolite imaging studies are 2,5-dihydroxybenzoic acid (DHB) and α-cyano-4-hydroxycinnamic acid (CHCA), while many new organic matrices have been developed to date including *N*-(1-naphthyl) ethylenediamine dinitrate,[31] 9-AA,[32] 1,5-diaminonaphthalene (1,5-DAN),[33] hydroxyflavones,[34] and *N*-(1-naphthyl) ethylenediamine dihydrochloride (NEDC).[35]

Compared to the classical crystalline matrices, ionic liquid matrices (ILM) have shown some advantages in producing more homogeneous sample spots and thus higher reproducibility.[36,37] ILM are equimolar mixtures of conventional matrices like DHB or CHCA combined with organic bases like pyridine (Py) or *N*,*N*-dimethylethylenediamine (DMED). Nanoparticles have also become attractive new matrix subjects. Silver,[38] TiO_2,[39,40] and gold[41] nanostructured materials have been successfully applied in surface assisted laser desorption/ionization mass spectrometry (SALDI MS). The results show that they simplify sample preparation, improve reproducibility of peak intensities for analytes, and eliminate background signals from matrix degradation. All of these properties make them useful matrices for the identification of small molecules. Graphene (G) has emerged as another novel matrix alternative for analysis of low mass compounds.[42] With recent advances in nanotechnology, G-based nanomaterials[43−45] have shown great improvements as a substrate for matrix-free LDI MS to detect and image diverse molecules with high sensitivity, with minimal background interference, especially in the low mass range.

Matrix application strategies range from spotting to sublimation methodologies. Direct spotting of matrix on tissue surfaces allows for excellent extraction of molecules but results in a lower lateral spatial resolution of around 200 μm and poor spot-to spot and shot-to-shot reproducibility. Matrix spraying using either an artistic airbrush or a robotic sprayer such as ImagePrep (Bruker Daltonics Inc.), SunCollect sprayer (SunChrom, Friedrichsdorf), and TM-Sprayer (HTX Technologies Inc.) offers a resolution between 10 and 20 μm, though wetting of the tissue will delocalize the drug of interest and also cause tissue shrinkage if spraying conditions are not carefully controlled. Sublimation is an alternative solvent-free technique to deposit high purity matrix directly on the sample while avoiding the possibility of analyte diffusion and spreading in the specimen. Sublimation and rehydration generates homogeneous small crystals of matrix, thus giving high image resolution, but has lower sensitivity for the analysis of lipids and small molecules. The solvent-free matrix dry-coating approach[46] can be another alternative way to overcome tissue shrinkage with improved matrix crystal distribution and enhanced signal uniformity. However, in this dry-coating method, extraction of analytes is less effective and molecules undergo limited ionization, especially in the case of pharmaceutical compounds. Both to obtain homogeneous matrix coverage and to improve ionization efficiency, the two-step matrix application

DOI: 10.1021/acs.analchem.5b00419
Anal. Chem. 2015, 87, 9508−9519

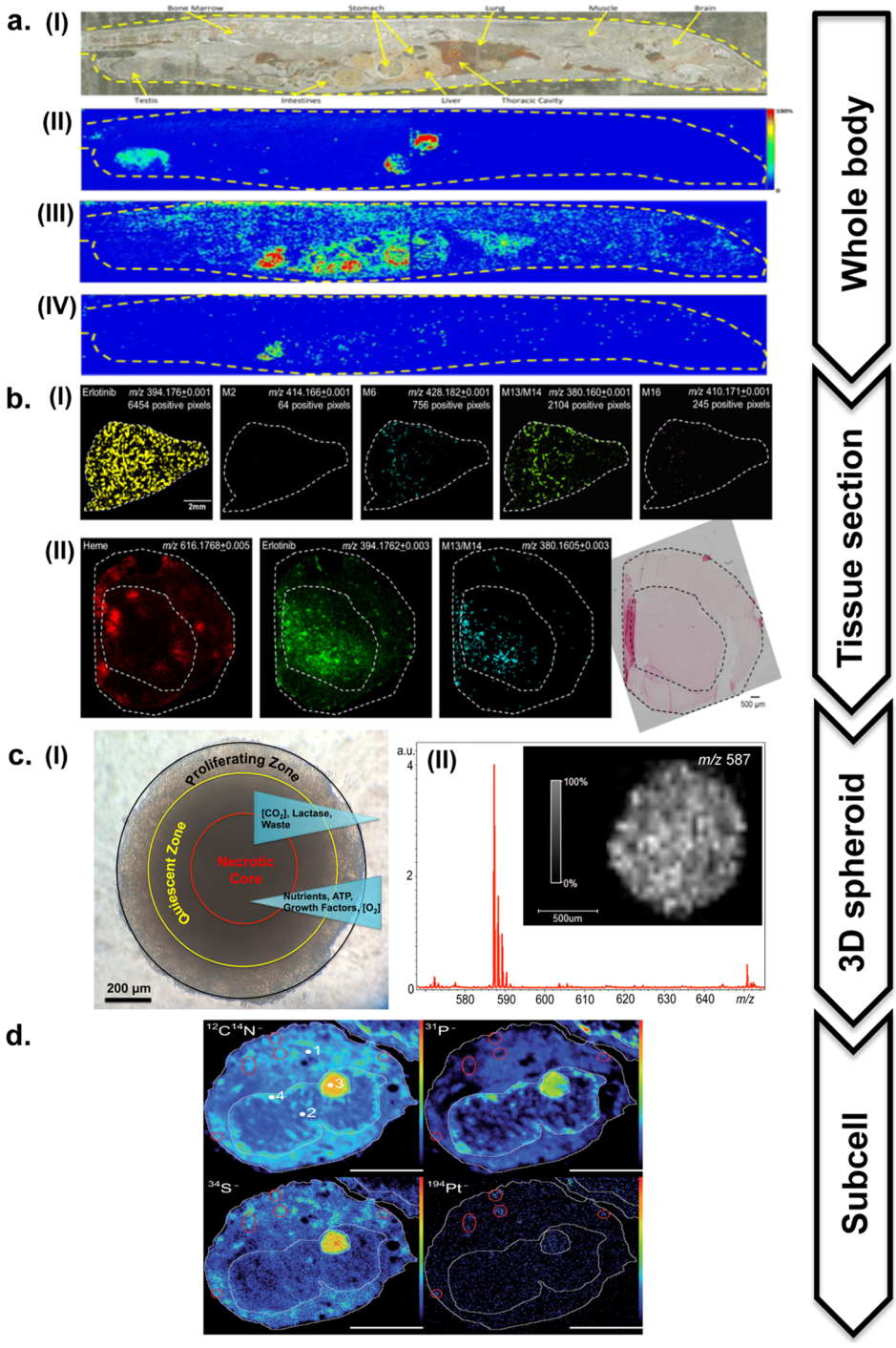

Figure 1. Mass spectrometry imaging technologies from whole body to subcellular level. (a) Extracted ion images at 5 ppm mass tolerance: [I] optical image of sagittal section of 20 mg/kg reserpine rat 2 h postdose; [II] reserpine (m/z 609.281); [III] methyl reserpate (m/z 415.223); [IV] reserpic acid (m/z 401.207). (b) MALDI FTICR MSI images of: [I] different metabolites from mouse liver treated with erlotinib under 60 μm resolution; [II] heme,erlotinib, and metabolites in mouse brain tissue (10 μm thickness) with U87 xenograft tumor. Images were acquired at 50 μm resolution for a total of 14 000 spectra, and sister sections were H&E stained. (c) Application of MALDI MSI in MCTS: [I] structure of MCTS; [II] localization of irinotecan within a 12 μm section of an irinotecan-treated (20.6 μM, 24 h) HCT 116 MCTS obtained by MALDI MSI. (d) Exemplary $^{12}C^{14}N^-$, $^{34}S^-$, $^{31}P^-$, and $^{194}Pt^-$ secondary ion signal intensity distribution maps acquired from semithin sections of SW480 cells treated with 25 μM of cisplatin. Regions of interest (ROIs) were manually defined within the cytoplasm, the nucleus, the nucleolus, and the chromatin. According to the $^{194}Pt^-$ and $^{34}S^-$ signals, the drug is accumulated in small cytoplasmic, sulfur-rich aggregates (encircled in red), as well as in the nucleoli. The scale bars are 5 μM. (a) Reprinted from ref 28. Copyright 2012 American Chemical Society. (b) Reprinted with permission from ref 56. Copyright 2013 Macmillan Publishers Ltd. (d) Reprinted with permission from ref 72. Copyright 2014 The Royal Society of Chemistry.

was developed. This approach employs the airbrush spaying or sublimation in the first step to produce small matrix crystals, followed by the deposition of droplets of matrix solution using automatic dispensers, or spraying to achieve recrystallization.[47−49] As a result, improved crystal morphology and size drastically enhances signal intensity, reproducibility, and imaging quality.

DOI: 10.1021/acs.analchem.5b00419
Anal. Chem. 2015, 87, 9508−9519

Therefore, it is also suggested that an appropriate matrix application method needs to be optimized for different biological tissue samples to achieve uniform matrix distribution, reduced crystal size, and controlled solvent effects.

The choices of matrix and application method are crucial steps to improve sensitivity and spatial resolution for specific analytes of interest. These advances in matrix types and application approaches greatly assist with the identification and mapping of drugs and metabolites in tissue samples. Careful optimization and planning of sample preparation before performing any large-scale analysis are necessary to generate high-quality MALDI-MSI data.

SPATIAL RESOLUTION

Spatial (lateral) resolution, or pixel resolution, generally refers to the center-to-center distance between spectra. While sample preparation factors like matrix crystal size or delocalization of analytes during matrix application contribute, the physical limitation of spatial resolution is also determined by the diameter of the laser beam.[8] Several instrumental approaches have been developed to improve the spatial resolution. One method involves the use of a 20 μm pinhole filter to reduce the diameter of the laser beam.[50] The spatial resolution was increased from 20 to 5 μm on two MALDI-TOF instruments with this approach. In other examples, a transmission geometry vacuum ion source was developed to provide submicrometer laser spot sizes by irradiating the backside of the sample,[51] while a Gaussian beam profile has been designed using optical single mode fibers to give a small laser beam diameter.[52] Oversampling is another method to improve spatial resolution. This approach involves using a raster increment smaller than the width of the laser beam coupled with complete matrix ablation so that only a fraction of the beam is generating the analyte signal. In this method, resolution is not limited to the size of the laser beam.

Spatial resolution is an important parameter to consider in the design of a therapeutic imaging experiment. For a whole body MSI study in rats, a spatial resolution of several hundred micrometers is sufficient to provide an overview of distribution patterns of drugs and metabolites in major organs or tissues with the advantage of speed (sample area/time) and sensitivity. A resolution between 20 and 200 μm can be used for MSI of specific tissues or organs, while a higher resolution (<20 μm) is necessary for imaging applications at the cellular level. Therefore, it is necessary to determine the proper spatial resolution needed to answer the question at hand before analyzing a sample. All of the developments in improving the spatial resolution will have great benefits for the MALDI-MSI analyses of therapeutics at the cellular and subcellular levels.

DETECTION AND IDENTIFICATION OF DRUGS AND METABOLITES

A great challenge for the identification of drugs and metabolites in biological samples is the interference caused by numerous endogenous species as well as the matrix ion signals. Detection of molecules with similar m/z values or overlapping isotopic clusters can lead to ambiguous molecular identification. There are several solutions to eliminate this interference. If the matrix peaks overlap with the m/z of the analytes of interest, the analyte signals can be unmasked by either deuterating the matrix to generate a mass shift[53] or substituting the matrix with an alternative substance. In other cases, the use of standards for drugs and major metabolites can aid in the development of a targeted imaging approach to increase analytical sensitivity for specific compounds. The use of imaging MS/MS to generate ion density maps for product ions, which are matched to those of the precursor ion, also increases confidence in the identification process. The rapid development of high resolving power as well as subppm mass accuracy MS instruments such as the Orbitrap[52] and FTICR[54−56] can also help differentiate peaks of similar mass. In Figure 1b, the high mass accuracy of FTICR acquisition (<1 ppm mass tolerance) gives a confident assignment and spatial distribution of the drug erlotinib, as well as its four metabolites, within the liver of a drug-treated mouse without requiring MS/MS. Recently, the application of ion mobility analyses enable a postionization separation step that assists in resolving peaks of isobaric species based on their distinct molecular cross sections. By incorporating this methodology, the drug vinblastine was successfully distinguished from endogenous lipid molecules in whole body rat sections.[57]

QUANTIFICATION

Quantification requires that the magnitude of the measured signal intensity is proportional to the concentration or amount of the analyte in the sample matrix. The relative quantitative information acquired from MALDI-MSI experiments should be taken with special consideration. Ion suppression, heterogeneity of target surface, matrix crystal size and morphology, ionization efficiency, stability of analytes, and fluctuations in detector response can all affect the results. One way to address such issues is the normalization of the drug signals to the total ion current or endogenous species.[58] However, uneven distribution of the endogenous species can lead to artifacts if the intensities of the pharmaceutical compounds are normalized against them. An alternative approach is to normalize to a homogeneously applied standard, which has similar properties and ionization efficiencies as the compound(s) being analyzed.[59] Compound signals that increase relative to that of the internal standard when different samples are compared can be considered to represent increases in the amounts of the analytes, while decreases reflect reduced levels. This approach has been shown to be an effective way to compensate for inherent variability in sample preparation and ionization process.

For absolute quantification, the measured ion intensities cannot be directly compared to an absolute quantity without a reference standard due to the reasons described above. To date, the majority of approaches for drug quantification using MALDI-MSI involve generating a standard curve for the compound by spotting a range of concentrations onto the surface of a control tissue section.[9] By comparing the ion intensities from the dosed sample, the drug concentration is then estimated. This is a quick and simple method; however, there are still limitations in terms of the uniformity of spotting standards for reproducibility and accurate reflection of the extraction efficiency of the drug in treated samples. To overcome this challenge, a novel method using a mimetic tissue model, including a set of tissue homogenates spiked with varying drug concentrations, has been employed.[60] The frozen model was sectioned and analyzed together with the dosed tissues. Differences in analyte extraction and ion suppression were taken into consideration in this methodology. Two drugs, lapatinib and nevirapine, were successfully quantified with this approach, and the results were comparable to the LC-MS quantification.

DOI: 10.1021/acs.analchem.5b00419
Anal. Chem. 2015, 87, 9508−9519

DATA PROCESSING, ANALYSIS, AND AVAILABLE SOFTWARE

Data processing, performed to find m/z values that correspond to analytes of interest (e.g., pharmaceutics and their metabolites), serves as a bridge between the raw data set and data visualization or analysis. The initial step in data analysis requires preprocessing: baseline correction, noise reduction, normalization, spectra smoothing, and recalibration, which allows cleaning of the spectra from baseline and background noise, facilitating the selection of peaks of interest.[61] The next step involves data representation using multivariate statistical analysis of the processed spectra and spatial segmentation based on clustering.[61,62]

Commercially available software for MALDI imaging data acquisition and visualization from vendors includes FlexImaging (Bruker Daltonics), HDI (Waters), ImageQuest (Thermo Scientific), TissueView (AB Sciex), Intensity Mapping (Shimadzu), and WinCadence (Physical Electronics). In addition to vendor-provided software, Biomap (Novartis) and Datacube Explorer V0.7 (AMOLF) can be used for visualization and basic statistical analysis. Other imaging generic tools, written in, e.g., ImageJ, or Matlab like OmniSpect, or MSiReader, have also been developed. Recently, an open-source R-based software package is available for processing and visualization of spectra, followed by statistical segmentation, such as Principal Component Analysis (PCA), Spatially Aware, and Spatial Shrunken Centroids segmentation methods, and classification with Partial Lease Squares Discriminant Analysis and Orthogonal Projections to Latent Structures Discriminant Analysis of the resulting images.[63] As well as the commercial imaging software packages, in-house developments for data analysis are excellent alternatives in the MALDI imaging field. Our lab recently developed an analysis pipeline within the MATLAB programming platform employing a combination of PCA, clustering methods, and linear discriminant analysis to visualize differences in protein expression levels across a 3D tumor spheroid section.[64] Due to the flexibility of the popular computing environment like MATLAB or R, such in-house developed analysis methods can be easily utilized and adapted by other researchers.

Overall, developments in sample preparation protocols, instrumentation, and data analysis have vastly improved the speed, spatial resolution, and sensitivity of MALDI-MSI, which is rapidly maturing as a routine bioanalytical technique with great potential for pharmaceutical discovery and development investigations.

OTHER MAJOR IONIZATION TECHNIQUES

To avoid matrix interference and simplify sample preparation procedures, matrix-free techniques have also been developed and applied in therapeutic MSI studies. Secondary ion mass spectrometry (SIMS) was one of the first matrix-free desorption/ionization methodologies for the analysis of metabolites.[65] SIMS uses a beam of high-energy primary ions to bombard and eject secondary ions from the sample surface, which are then guided into the mass spectrometer for analysis. SIMS MSI can be divided into two categories, static and dynamic SIMS. Static SIMS has a low primary-ion count resulting in about 1% of the uppermost surface monolayer being sampled, while in the dynamic mode, high primary ion current densities are used to sample all of the upper monolayers of the surface.[66] SIMS typically desorbs and ionizes small molecules and has high spatial resolution (down to 50 nm) to reach subcellular levels for imaging.[67] SIMS MSI instruments can also perform depth-profiling experiments with depth resolution greater than 50 nm by an erosive process of sputtering with the primary-ion beam to determine the molecular localizations beneath the sample surface and consequently enabling 3D imaging. Although SIMS possesses high spatial resolution, it suffers from limited sensitivity at >500 Da and extensive surface fragmentation generated by high-energy primary ions[68] making it unpopular for tissue samples. However, used in combination with other techniques, such as MALDI-MSI[1], scanning electron microscopy,[69] atomic force,[70] or fluorescence microscopy,[71] SIMS has great potential to expand its application in therapeutic studies. Recently, an advanced type of dynamic SIMS, nanoscale SIMS combined with confocal laser-scanning microscopy, was designed for trace element and isotope analysis.[72] It was successfully applied for subcellular mapping of metal-based compounds like platinum (Pt) complexes in cell culture samples exposed to cisplatin (Figure 1d).[72]

Siuzdak and co-workers first demonstrated nanostructure-initiator mass spectrometry (NIMS) in 2007.[73] NIMS is another matrix-free ionization technique with simple sample preparation using a liquid initiator to facilitate desorption.[73] During ionization, the nanostructured surface absorbs the laser energy, resulting in rapid surface heating, thus causing vaporization of the trapped initiator and triggering desorption of the absorbed analytes without fragmentation.[74] NIMS was shown to be sensitive for the localization of clozapine and its metabolite *N*-desmethylclozapine from rat brain sections.[75] More recently, it was used to detect intracellular uptake of 3′-deoxy-3′-fluorothymidine (FLT) and rapamycin, drug metabolism (FLT conversion to FLT-monophosphate), and downstream pharmacodynamic responses at the level of single lymphoma cells.[76] This relatively new matrix-free approach provides soft ionization, molecular specificity, high sensitivity, and high cell-level spatial resolution, which are important criteria in pharmaceutical studies and in optimization of existing therapies.

Several ambient ionization techniques have also been introduced and utilized in MSI studies of drugs and metabolites. Desorption electrospray ionization (DESI) is one such technique. It is performed by the interaction of charged droplets with a surface, producing gaseous ions that are directed into the mass spectrometer by use of an ion transfer line.[77] This method has been used on several occasions for the imaging of drugs like clozapine[78,79] and propranolol[80] in rat tissue sections and whole mouse bodies. However, the poor spatial resolution of ∼250 μm for DESI limits its application. Recent improvements in sprayer flow rate, sprayer surface angle, and sprayer diameter[81] have enhanced the resolution to less than 50 μm. Currently, development of nano-DESI has achieved a spatial resolution of 20 μm while analyzing small molecules across rat brain tissue.[82]

Liquid extraction surface analysis (LESA) is also an ambient solvent-based ionization method. In LESA, a droplet of solvent is placed on the sample at a specific position to extract analytes, followed by electrospray ionization. Currently, LESA lacks high spatial resolution. The spatial resolution is limited by the size of the pipet nozzle to deposit and aspirate the extraction solvent, and typically, 1 mm diameter is sampled.[83] However, it does not require additional sample preparation and has high sensitivity when used in selected reaction monitoring mode. It has been used as a rapid complementary technique to MALDI-MSI when detailed spatial distribution is not necessary. LESA has been applied to map the distribution of drugs like terfenadine,[83] moxifloxacin,[84] chloroquine, and its metabolites[85] in sections from whole body, organs or tissues of rat, and the data was validated against WBA, DESI, or MALDI-MSI approaches. In other studies, LESA MSI also enabled semiquantification of drugs and their metabolites, and the results correlated with quantitative WBA data.[86,87]

DOI: 10.1021/acs.analchem.5b00419
Anal. Chem. 2015, 87, 9508−9519

Similar to DESI, laser ablation ESI (LAESI) is another ambient ionization technique that is less destructive to the sample surfaces under investigation.[88] LAESI employs a mid-IR laser beam at 2940 nm. The IR laser beam excites the hydroxyl vibrations of water molecules and ablates the surface in concert with electrospray ionization.[88] LAESI was first introduced by Nemes and Vertes in 2007[88] and used in biomedical imaging in 2010.[89] So far, it has been used to map lipids and metabolites in animal organs,[89,90] and this approach has great potential to be applied in pharmaceutical imaging studies.

Laser ablation inductively coupled mass spectrometry (LA-ICPMS) has been developed for the evaluation of metal containing compounds. Using LA-ICPMS, it is possible to visualize the distribution of metals deriving from metallo-drugs, such as the Br-containing drug TMC207,[91] gold compounds,[92] and platinum drugs like oxaliplatin,[93] cisplatin,[94−96] and carboplatin[97] in mouse tissue. This method achieves spatial resolution at subcellular levels[96] and also enables quantification of metal complexes.[97] One disadvantage of this technique is the limited detection capability; the approach is specific for compounds containing metals. Combining it with other methodologies can expand its application in drug discovery and development.[98] Advantages and limitations of the various ionization approaches are summarized in Table 1.

A NOVEL APPLICATION: 3D CELL CULTURE SYSTEMS

Cell cultures have been proven to be indispensible during the drug development process for preanimal and preclinical evaluation of promising therapeutics. For decades, most studies testing drug candidates were performed using the cells of interest cultured on compatible polystyrene in a two-dimensional (2D) monolayer format. 2D cell monolayers provide a well-controlled and homogeneous cellular environment, simplify the analysis techniques, and sustain the growth and proliferation for most cell types. However, the results from this in vitro system have been questioned for not accurately recapitulating in vivo scenarios due to differences in cell morphology, proliferation, gene expression patterns, and cell−cell or cell−matrix interactions.[99−103] In addition, from a drug delivery perspective, 2D cell cultures also lack the appropriate physiological barriers arranged in a proper geometry to mimic the microenvironment in the body.[99]

Alternatively, attention has shifted to 3D cell cultures, using scaffolds, hydrogel, and microfabricated devices to provide enhanced models to more closely replicate the complex in vivo conditions for testing of drug delivery, metabolism, and toxicity.[99] Among the different 3D cell culture systems, multicellular tumor spheroids (MCTS), which are spherical self-assembled cell clusters, are one of the most commonly used models that closely mimic human solid tumors.[104] Figure 1c (I) shows a typical structure of a MCTS with a radius greater than 200 μm. Because of oxygen and nutrient diffusion limits, all cells and metabolic waste accumulate within the tumor mimics. The large MCTS harbor concentrically layered zones of highly proliferative cells on the outer rim, quiescent cells on the inside, and necrotic cells at the core region. This heterogeneous system reflects the in vivo microenvironment of proliferating tumor cells next to capillaries, while more distant cells stay quiescent or die through apoptosis.

Similar to in vivo tissues, MCTS show greater resistance than single cells or monolayer cultures to a given dose of many pharmaceuticals.[105−109] This phenomena was first demonstrated by Durand and Sutherland in 1972[109] and later termed "multicellular resistance (MCR)"[110] and replicates a significant obstacle to successful cancer therapy. Factors causing MCR include: intercellular molecular changes like activation of Stat3 and NF-κB signaling pathways, microenvironment alterations like changes in extracellular matrix (ECM) and varying pH, the presence of hypoxic cells, differences in cell cycle distribution within MCTS and, importantly, drug penetration within spheroids, which is the rate-limiting step for drug delivery.[104,111,112] In addition to structural and physical properties, poor penetration of drug molecules into spheroids can be caused by binding with the outer layers of cells or physical barriers due to the ECM and cellular membranes.[108,113,114] Additionally, pH gradients within the 3D structure sometimes protect cells in the acidic core from weakly acidic compounds such as mitoxantrones, while enhancing the effect of weakly basic drugs such as chlorambucil.[115] Due to the inherent pathophysiological gradients, the heterogeneous structure, and transport limitations, MCTS are an accurate model to evaluate therapeutics, especially drug penetration limitations and metabolism properties. Nevertheless, methodologies for imaging drug distribution in spheroids were limited to approaches that required labels like fluorescent microscopy[116,117] or autoradiography.[118] More convenient and powerful methods for direct localization of drugs and their metabolites are still in great need.

In early 2011, a MALDI-MSI experiment on a 3D reconstructed skin tissue model was established to study the absorption of imipramine into skin.[119] Months later, the Hummon laboratory was the first to adapt this complementary label-free MALDI-MSI in 3D MCTS.[120] This methodology was originally performed in colon adenocarcinoma HCT 116 spheroids for mapping the distribution of proteins,[120] and then further applied to study the penetration of the anticancer drug irinotecan [Figure 1c (II)].[121] A typical MALDI-MSI workflow for therapeutic evaluation in MCTS is shown in Figure 2. Spheroids are grown to ∼1 mm in diameter on an agarose-coated 96-well plate. Around day 13, MCTS are large enough to exhibit chemical gradients and cellular heterogeneity and thus are ready to be dosed with pharmaceutical compounds. After a specific length of treatment time, spheroids are gently transferred with a seratological pipet and embedded in gelatin. The frozen gelatin block containing the MCTS is then sectioned at thicknesses between 10 and 14 μm on a cryostat and thaw-mounted to ITO coated glass slides. After application of an appropriate matrix, MALDI-MSI is then performed for the spatial localization of drugs and metabolites. For more details and a video of this protocol, please consult Ahlf Wheatcraft et al.[122]

With this methodology, the distribution of irinotecan (m/z 587) has been imaged in HCT 116 MCTS after 20.6 μM treatment for specified lengths of time. Irinotecan accumulation in the periphery and the center of spheroids increases with time as shown by ion density maps in Figure 3. In the first 6 h of incubation, irinotecan was present only in the periphery, followed by an enhanced drug penetration into the central part of the spheroids within 12 h. After 24 h of treatment, irinotecan was distributed across the entire structure of the MCTS, with areas of drug accumulation evident at 48 h of treatment. The identities of the irinotecan metabolites were examined by nanoflow liquid chromatography-tandem mass spectrometry (nLC-MS/MS). By analyzing the small molecules extracted from the drug-treated spheroids, ten metabolites in total were identified. MALDI-MSI provides sensitive image analysis of not only the parent drug but also the metabolites simultaneously. Three metabolites, including the bioactive metabolite SN-38, were also mapped in treated spheroids after 72 h of drug incubation.

DOI: 10.1021/acs.analchem.5b00419
Anal. Chem. 2015, 87, 9508−9519

Table 1. Overview of Various Ionization Techniques for Imaging Mass Spectrometry Analysis

technique		mass range (Da)	lateral resolution (μm)	advantages	limitations	commercialized by
MALDI		0−70 000	30−500	soft ionization; wide mass range; atmospheric pressure and vacuum sources available; high tolerance of sample (size, shape, salts, and detergents); versatile method	molecular coverage and imaging quality depend on matrix; quantitative analysis is challenging; interference with matrix-related peaks below m/z = 300	Bruker Daltonics; Shimadzu; Thermo Fischer Scientific; Waters; Applied Biosystems; AB Sciex
SIMS	static mode	0−2000	0.5−50	high spatial resolution; wealth of molecular information; low consumption of material; various primary-ion guns available	source-induced fragmentation; small sampling area; low signal levels; very high surface sensitivity; samples must be compatible with an ultra high vacuum	Physical Electronics; IonTOF
	dynamic mode	0−300	0.04−0.5	very high spatial resolution (cellular and subcellular level); high signal intensity for ppb-level elemental analysis; quantitative imaging possible; depth profiling possible	limited molecular information; risk of tissue damage; small sampling area; very high surface sensitivity; samples must be compatible with ultra high vacuum; few ions can be measured simultaneously	Cameca; Physical Electronics; Millbrook Instruments
NIMS		0−1500	15−20	soft ionization; no sample preparation; low chemical noise and high sensitivity in the low mass range below 1000 m/z; flexibility of different initiators	risk of tissue slice damage during imaging process; surface modifications/additives are needed to improve ionization efficiencies	not yet commercialized
DESI		0−5000	100−1000	soft ionization; no sample preparation; ambient ionization technique	low spatial resolution; molecular coverage depends on spray composition; risk of destroying samples with high-pressure gas	Prosolia
LESA		0−2000	∼1000	no sample preparation; high sensitivity of detection due to efficiency of surface extraction method	low spatial resolution limits the investigation of smaller regions within biological structure of interest; surface needs to be sufficiently hydrophobic to form a micro liquid junction between tip and sample	Advion
LAESI		0−66 000	200−400	minimal sample preparation; depth profiling possible	low spatial resolution; water rich target is needed for ablation process; variations of water content and tensile strength can affect ion yield and imaging results	Protea Biosciences
LA-ICP		6−250	5−200	simultaneous determination of all trace, minor, and major elements and isotopes in tissue; depth profiling possible; quantitative imaging possible; excellent for metal analysis; low danger of contamination	invasive technique; isobaric or multiply charged elements at same nominal mass can interfere with atomic ions of analytes; reference materials with similar matrix composition required for quantification	Waters; Thermo Fischer Scientific; Applied Spectra; Agilent Technologies

DOI: 10.1021/acs.analchem.5b00419
Anal. Chem. 2015, 87, 9508−9519

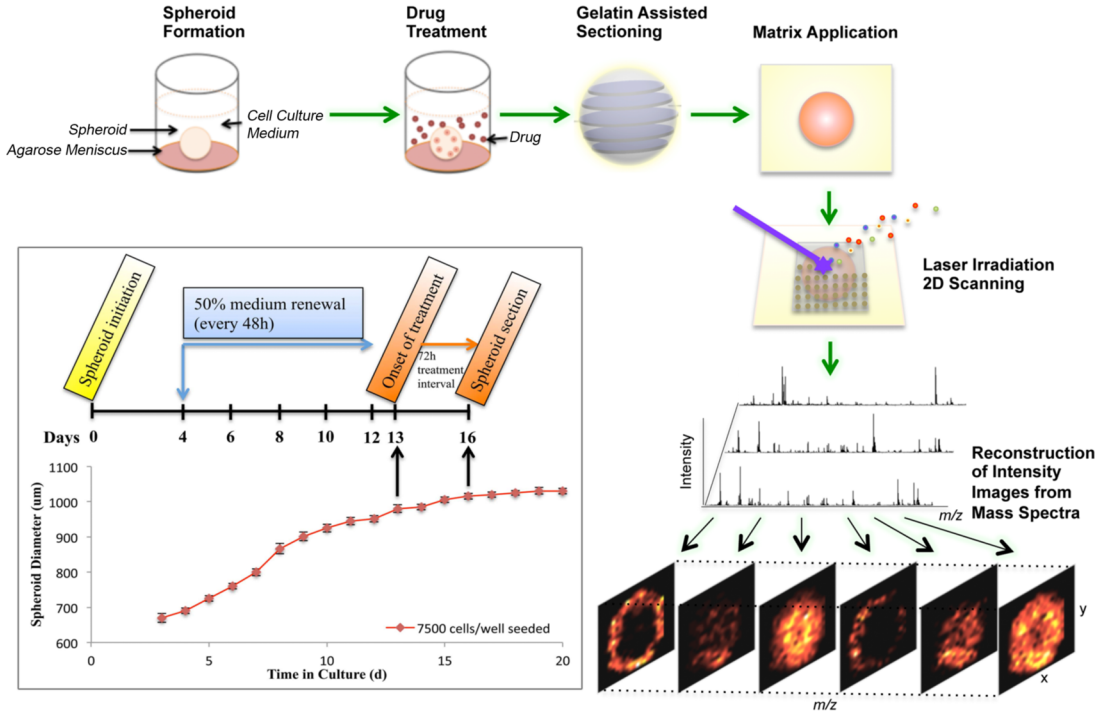

Figure 2. General scheme of MALDI MSI technology in 3D cell cultures for evaluation of therapeutics. Cells are seeded in agarose-coated 96-well plate for MCTS formation. When MCTS grow to ∼1 mm in diameter, which is large enough for establishing cellular heterogeneity and chemical gradients to mimic in vivo tumors, they are ready to be treated with pharmaceutical compounds. After a specific time length, MCTS are gently collected and embedded in gelatin for sectioning, followed by MALDI-MSI analysis. This workflow enables simultaneous localization of drugs and metabolites in the MCTS sample without needing any prelabeling. Left bottom panel reprinted from ref 121. Copyright 2013 American Chemical Society.

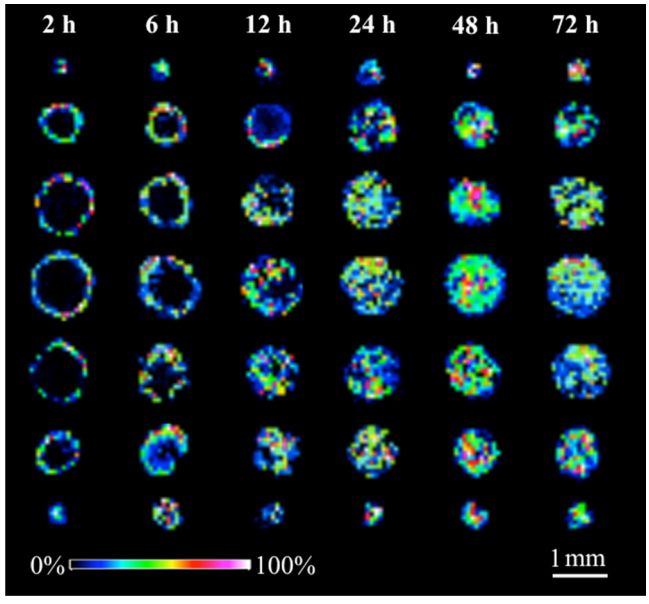

Figure 3. Time-dependent penetration of irinotecan (m/z 587) in HCT 116 MCTS analyzed by MALDI-IMS. MCTS were treated with 20.6 μM irinotecan for 2, 6, 12, 24, 48, and 72 h (from left to right). For every treatment duration, color gradient intensity maps were generated from 7 consecutive, 12 μm slices from a single MCTS in 120 μm vertical intervals. Reprinted from ref 121. Copyright 2013 American Chemical Society.

This approach is valuable in assessing delivery of irinotecan and other various pharmaceutical entities in MCTS. Leucovorin or folinic acid is converted in vivo into the biologically active metabolite folate and enhances the effect of 5-fluorouracil (5-FU) in colorectal cancer. 5-FU is metabolized to the active metabolite 5-fluoro-2′-deoxyuridine 5′-monophosphate (FdUMP), binding to and inhibiting the enzyme thymidylate synthase (TS).[123] Folinic acid is rapidly metabolized to 5,10-methylenetetrahydrofolate (5,10-CH_2-THF), 5,10-methenyltetrahydrofolate (5,10-CH═THF), and then to 5-methyltetrahydrofolate (5-MTHF).[123,124] Leucovorin has no intrinsic antitumor effect, but its metabolite 5,10-CH_2-THF forms an inhibitory ternary complex with FdUMP and TS, which enhances the inhibition of thymidylate synthesis and impairment of both DNA synthesis and repair processes.[124] Figure 4 shows the penetration of folinic acid into MCTS after incubation with the compound at the concentration of 35 μM. Folinic acid (m/z 474) reaches and accumulates around the core region after 24 h of treatment. The metabolite 5,10-CH═THF (m/z 456) is also detected and found to be concentrated at the center of MCTS. It has been shown that folinic acid can be avidly converted into 5,10-CH═THF at acidic pH and this metabolite has great stability in low pH conditions.[125,126] Thus, the pH gradient of the MCTS could be a reason for this accumulation. The structures of both the folinic acid and 5,10-CH═THF have been confirmed by MALDI MS/MS.

MALDI-MSI is also compatible with other techniques like confocal Raman microscopy (CRM).[127] This correlated imaging approach was developed to evaluate the structural and chemical diversities of various molecules within the MCTS. CRM is a nondestructive imaging approach and enables subcellular visualization of classes of biomolecules, while MSI allows the identification and localization of small molecules from discrete regions of a spheroid section. Thus, different chemical data can be obtained and correlated to further investigate cellular

DOI: 10.1021/acs.analchem.5b00419
Anal. Chem. 2015, 87, 9508−9519

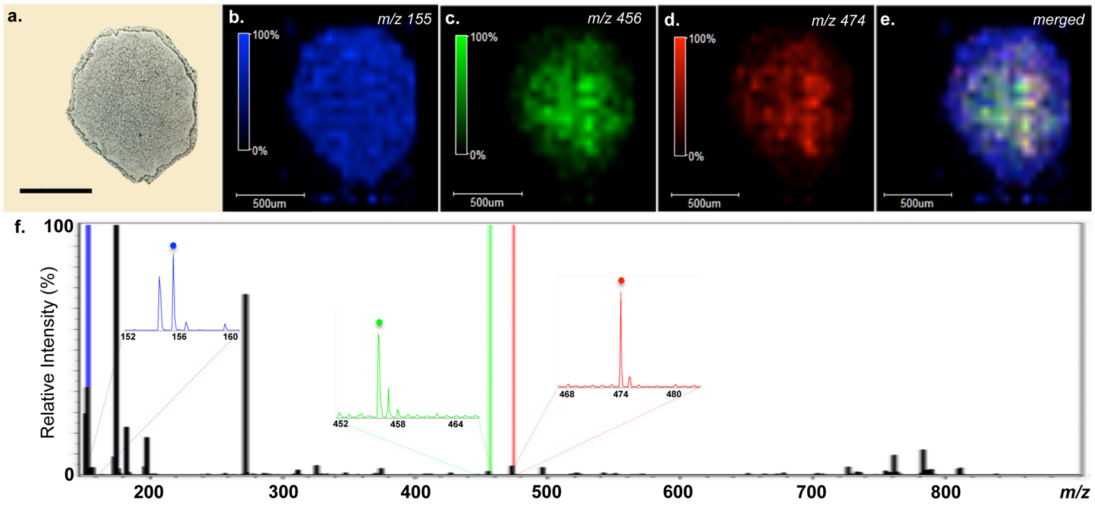

Figure 4. Distributions of folinic acid and one metabolite within a 12 μm section of an leucovorin-treated (35 μM, 24 h) HCT 116 MCTS obtained by MALDI-imaging. (a) Optical image of the MCTS section. Spatial localizations of (b) DHB (m/z 155, blue); (c) 5,10-CH═THF metabolite (m/z 456, green); (d) folinic acid (m/z 474, red). (e) Merged image shows high relative abundance of folinic acid. (f) Mass-to-charge plot.

responses to chemotherapeutical treatment as well as studying drug penetration and metabolism.

Recently, nanoparticle-assisted LA-ICPMS analysis of drug delivery in 3D cell cultures was performed.[128] Figure 5 shows the

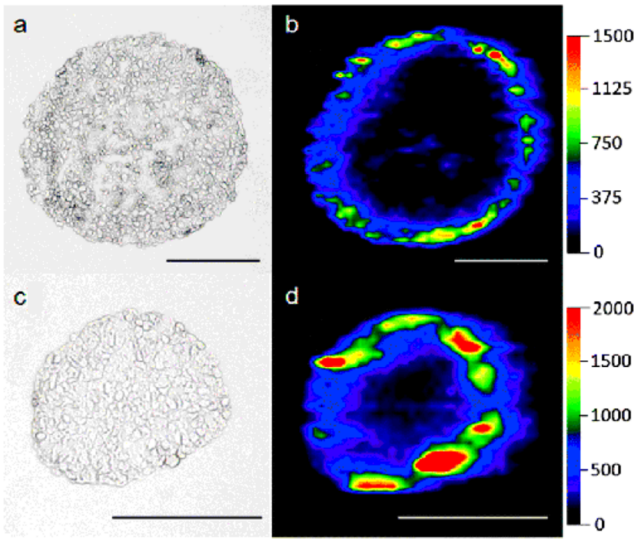

Figure 5. Images of TFK-1 tumor MCTS sections incubated with mTHPP-PdPLGA nanoparticles for 48 h [(a) + (b)] 8.2 μg/mL and [(c) + (d)] 40.7 μg/mL. The scale represents a length of 200 μm in all images. The ^{105}Pd signal is used for data evaluation. Intensity is stated in counts per second (cps). Images were obtained using a laser spot diameter of 10 μM. Reprinted with permission from ref 128. Copyright 2014 The Royal Society of Chemistry.

images acquired from the TFK-1 MCTS incubated for 48 h with 8.2 μg/mL [(a) + (b)] and 40.7 μg/mL [(c) + (d)] 5,10,15,20-tetrakis(3-hydroxy-phenyl)porphyrin (mTHPP) loaded poly(lactic-*co*-glycolic acid) (PLGA) nanoparticles. mTHPP is a second-generation photosensitizer and was tagged by complexing with palladium before analysis. The results show that a distinct enrichment of the drug occurs predominantly within the outer layers of the spheroids, which could be attributed to the very high affinity of the low polarity compounds to proteins. This work proves the LA-ICPMS as another promising approach to study penetration of metal containing drugs into MCTS.

Together, these combinations of powerful label-free MSI techniques with 3D MCTS have great possibility to improve the predictive power for in vivo therapeutic efficacy. Not only can drug penetration be evaluated, but the drug metabolism and distribution of various analytes can also be studied simultaneously. These methodologies provide significant benefits for MCTS to become an essential screening tool for the preclinical assessment of a variety of therapeutics.

CONCLUSIONS

Recent developments of MSI in the arena of drug and metabolite localization have revealed great potential for pharmaceutical discovery processes. MALDI-MSI remains a popular approach due to its high sensitivity and simplicity of operation. Advances from sample preparation to instrumentation have vastly improved the speed, selectivity, spatial resolution, and identification capabilities for MSI by MALDI. Other well-developed ionization methods like SIMS, NIMS, DESI, LESA, LAESI, and LA-ICP ensure a variety of options for mapping drugs and metabolites in various tissue or organ samples with different spatial resolutions.

Testing of pharmaceutical compounds in 3D cell cultures is increasingly regarded as an essential step during drug development. Application of MALDI-MSI and LA-ICP techniques in MCTS has shown great advantages for directly and rapidly imaging the distribution of both parent drug and multiple metabolites in a single experiment. With further optimization, it is expected that other ionization methods will have greater roles to play for drug evaluation in 3D cell cultures. In addition, colocalization of pharmaceuticals with proteins, metabolites, or lipids in MCTS using MSI could be another possibility to acquire more useful information on therapeutic response directly at the action site of a drug. Moreover, future work should be directed toward combinatorial therapy studies in this model system.

By adapting MSI technologies, MCTS will become a more powerful and informative platform to screen and select drugs in a format that closely mimics the microenvironment conditions in patients. With continued developments in MSI, this system also has great potential to be a common and routine approach in the drug discovery and development workflow.

DOI: 10.1021/acs.analchem.5b00419
Anal. Chem. 2015, 87, 9508−9519

AUTHOR INFORMATION

Corresponding Author

*E-mail: ahummon@nd.edu. Phone: 574-631-0583. Fax: 574-631-6652.

Notes

The authors declare no competing financial interest.

Biographies

Xin Liu is a Ph.D. student in Amanda B. Hummon's lab at University of Notre Dame. She received her B.S. from Nankai University, and her research is focused on using mass spectrometric techniques to evaluate penetration and metabolism of pharmaceutical compounds in 3D cell culture systems.

Amanda B. Hummon is the Charles L. Huisking Associate Professor in the Department of Chemistry and Biochemistry at the University of Notre Dame. She received an AB from Cornell University and a Ph.D. in Chemistry from the University of Illinois at Urbana−Champaign. Her research group develops analytical methods to evaluate both the transcriptome and proteome to understand colorectal cancer systems and is also working on establishing high-throughput approaches to analyze drugs and metabolites in 3D cell culture systems using mass spectrometry.

ACKNOWLEDGMENTS

We would like to thank Dr. Susan Skube for assistance with manuscript editing. This report was supported by the National Science Foundation (CAREER Award CHE-1351595) and the National Institutes of Health (1R01GM110406-01) for A.B.H. X.L. was supported by the Notre Dame Chemistry Biochemistry Biology Interface (CBBI) program and NIH Training Grant T32 GM075762. The Walther Cancer Foundation provided salary support for A.B.H.

REFERENCES

(1) Solon, E. G.; Schweitzer, A.; Stoeckli, M.; Prideaux, B. *AAPS J.* **2010**, *12*, 11−26.
(2) Markus, P.; Vernaleken, I.; Roesch, F. *J. Med. Chem.* **2014**, *57*, 9232−9258.
(3) Chu, P. C.; Chai, W. Y.; Hsieh, H. Y.; Wang, J. J.; Wey, S. P.; Huang, C. Y.; Wei, K. C.; Liu, H. L. *Biomed. Res. Int.* **2013**, 627496.
(4) Panthani, M. G.; Khan, T. A.; Reid, D.; Hellebusch, D. J.; Rasch, M. R.; Maynard, J. A.; Korgel, B. A. *Nano Lett.* **2013**, *13*, 4294−4298.
(5) Solon, E. G. *Chem. Res. Toxicol.* **2012**, *25*, 543−555.
(6) McEwen, A. B.; Henson, C. M.; Wood, S. G. *Bioanalysis* **2014**, *6*, 377−391.
(7) Meikle, S. R.; Beekman, F. J.; Rose, S. E. *Drug Discovery Today Technol.* **2006**, *3* (2), 187−94.
(8) Chughtai, K.; Heeren, R. M. A. *Chem. Rev.* **2010**, *110*, 3237−3277.
(9) Sun, N.; Walch, A. *Histochem. Cell Biol.* **2013**, *140*, 93−104.
(10) Prideaux, B.; Stoeckli, M. *Proteomics* **2012**, *75*, 4999−5013.
(11) Lietz, C. B.; Gemperline, E.; Li, L. *Adv. Drug Delivery Rev.* **2013**, *65*, 1074−1085.
(12) Greer, T.; Sturm, R.; Li, L. *J. Proteomics* **2011**, *74*, 2617.
(13) Ait-Belkacem, R.; Sellami, L.; Villard, C.; DePauw, E.; Calligaris, D.; Lafitte, D. *Trends Biotechnol.* **2012**, *30*, 466−474.
(14) Weaver, E. M.; Hummon, A. B. *Adv. Drug Delivery Rev.* **2013**, *65*, 1039−1055.
(15) Cornett, D. S.; Reyzer, M. L.; Chaurand, P.; Caprioli, R. M. *Nat. Methods* **2007**, *4*, 828.
(16) Reyzer, M. L.; Caprioli, R. M. *Curr. Opin. Chem. Biol.* **2007**, *11*, 29.
(17) Castellino, S.; Groseclose, M. R.; Wagner, D. *Bioanalysis* **2011**, *3* (21), 2427−2441.
(18) Norris, J. L.; Caprioli, R. M. *Chem. Rev.* **2013**, *113*, 2309−2342.
(19) Gessel, M. M.; Norris, J. L.; Caprioli, R. M. *J. Proteomics* **2014**, *107*, 71−82.
(20) Troendle, F.; Reddick, C.; Yost, R. A. *J. Am. Soc. Mass Spectrom.* **1999**, *10*, 1315.
(21) Reyzer, M. L.; Hsieh, Y.; Ng, K.; Korfmacher, W. A.; Caprioli, R. M. *J. Mass Spectrom.* **2003**, *38*, 1081−1092.
(22) Hsieh, Y.; Casale, R.; Fukuda, E.; Chen, J. W.; Knemeyer, I.; Wingate, J.; Morrison, R.; Korfmacher, W. *Rapid Commun. Mass Spectrom.* **2006**, *20*, 965−972.
(23) Signor, L.; Varesio, E.; Staack, R. F.; Starke, V.; Richter, W. F.; Hopfgartner, G. *J. Mass Spectrom.* **2007**, *42*, 900−909.
(24) Khatib-Shahidi, S.; Andersson, M.; Herman, J. L.; Gillespie, T. A.; Caprioli, R. M. *Anal. Chem.* **2006**, *78*, 6448.
(25) Hamm, G.; Bonnel, D.; Legouffe, R.; Pamelard, F.; Delbos, J. M.; Bouzom, F.; Stauber, J. *J. Proteomics* **2012**, *75*, 4952.
(26) Bouslimani, A.; Bec, N.; Glueckmann, M.; Hirtz, C.; Larroque, C. *Rapid Commun. Mass Spectrom.* **2010**, *24*, 415.
(27) Chen, J.; Hsieh, Y.; Knemeyer, I.; Crossman, L.; Korfmacher, W. A. *Drug Metab. Lett.* **2008**, *2*, 1.
(28) Shahidi-Latham, S. K.; Dutta, S. M.; Prieto-Conaway, M. C.; Rudewicz, P. J. *Anal. Chem.* **2012**, *84*, 7158.
(29) Shimma, S.; Sugiura, Y. *Mass Spectrom.* **2014**, *3*, S0029.
(30) Shariatgorji, M.; Källback, P.; Gustavsson, L.; Schintu, N.; Svenningsson, P.; Goodwin, R. J.; Andren, P. E. *Anal. Chem.* **2012**, *84*, 4603−4607.
(31) Chen, R.; Xu, W. J.; Xiong, C. Q.; Zhou, X. Y.; Xiong, S. X.; Nie, Z. X.; Mao, L. Q.; Chen, Y.; Chang, H. C. *Anal. Chem.* **2012**, *84*, 465−469.
(32) Shroff, R.; Muck, A.; Svatos, A. *Rapid Commun. Mass Spectrom.* **2007**, *21*, 3295−3300.
(33) Kim, Y. H.; Fujimura, Y.; Hagihara, T.; Sasaki, M.; Yukihira, D.; Nagao, T.; Miura, D.; Yamaguchi, S.; Saito, K.; Tanaka, H.; Wariishi, H.; Yamada, K.; Tachibana, H. *Sci. Rep.* **2013**, 32805.
(34) Wang, X.; Han, J.; Chou, A.; Yang, J.; Pan, J.; Borchers, C. H. *Anal. Chem.* **2013**, *85*, 7566−7573.
(35) Wang, J.; Qiu, S.; Chen, S.; Xiong, C.; Liu, H.; Wang, J.; Zhang, N.; Hou, J.; He, Q.; Nie, Z. *Anal. Chem.* **2015**, *87*, 422−30.
(36) Tholey, A.; Heinzle, E. *Anal. Bioanal. Chem.* **2006**, *386* (1), 24−37.
(37) Bonnel, D.; Franck, J.; Mériaux, C.; Salzet, M.; Fournier, I. *Anal. Biochem.* **2013**, *434* (1), 187−198.
(38) Hayasaka, T.; Goto-Inoue, N.; Zaima, N.; Shrivas, K.; Kashiwagi, Y.; Yamamoto, M.; Nakamoto, M.; Setou, M. *J. Am. Soc. Mass Spectrom.* **2010**, *21*, 1446−1454.
(39) Shrivas, K.; Hayasaka, T.; Sugiura, Y.; Setou, M. *Anal. Chem.* **2011**, *83*, 7283−7289.
(40) Moosi, L.; Spinelli, P.; Zucchetti, M.; Pretto, F.; Carrà, A.; D'Incalci, M.; Giavazzi, R.; Davoli, E. *PLoS One* **2013**, *8*, No. e72532.
(41) Amendola, V.; Litti, L.; Meneghetti, M. *Anal. Chem.* **2013**, *85* (24), 11747−11754.
(42) Dong, X.; Cheng, J.; Li, J.; Wang, Y. *Anal. Chem.* **2010**, *82*, 6208−6214.
(43) Kim, Y. K.; Na, H. K.; Kwack, S. J.; Ryoo, S. R.; Lee, Y.; Hong, S.; Hong, S.; Jeong, Y.; Min, D. H. *ACS Nano* **2011**, *5*, 4550−4561.
(44) Lu, M.; Lai, Y.; Chen, G.; Cai, Z. *Anal. Chem.* **2011**, *83*, 3161−3169.
(45) Qian, K.; Zhou, L.; Liu, J.; Yang, J.; Xu, H. Y.; Yu, M. H.; Nouwens, A.; Zou, J.; Monteiro, M. J.; Yu, C. Z. *Sci. Rep.* **2013**, *3*, 1415.
(46) Puolitaival, S. M.; Burnum, K. E.; Cornett, D. S.; Caprioli, R. M. *J. Am. Soc. Mass Spectrom.* **2008**, *19*, 882.
(47) Sugiura, Y.; Shimma, S.; Setou, M. *Anal. Chem.* **2006**, *78*, 8227.
(48) Ferguson, L.; Bradshaw, R.; Wolstenholme, R.; Clench, M.; Francese, S. *Anal. Chem.* **2011**, *83*, 5585−5591.
(49) Shimma, S.; Takashima, Y.; Hashimoto, J.; Yonemori, K.; Tamura, K.; Hamada, A. *J. Mass Spectrom.* **2013**, *48*, 1285−1290.
(50) Zavalin, A.; Yang, J.; Caprioli, R. *J. Am. Soc. Mass Spectrom.* **2013**, *24*, 1153−1156.
(51) Zavalin, A.; Todd, E. M.; Rawhouser, P. D.; Yang, J.; Norris, J. L.; Caprioli, R. M. *J. Mass Spectrom.* **2012**, *47*, 1473.
(52) Qiao, H.; Spicer, V.; Ens, W. *Rapid Commun. Mass Spectrom.* **2008**, *22*, 2779−2790.

DOI: 10.1021/acs.analchem.5b00419
Anal. Chem. 2015, 87, 9508−9519

(53) Shariatgorji, M.; Nilsson, A.; Goodwin, R. J. A.; Svenningsson, P.; Schintu, N.; Banka, Z.; Kladni, L.; Hasko, T.; Szabo, A.; Andren, P. E. *Anal. Chem.* **2012**, *84*, 7152−7157.
(54) Rompp, A.; Guenther, S.; Schober, Y.; Schulz, O.; Takats, Z.; Kummer, W.; Spengler, B. *Angew. Chem., Int. Ed.* **2010**, *49*, 3834−3838.
(55) Cornett, D. S.; Frappier, S. L.; Caprioli, R. M. *Anal. Chem.* **2008**, *80*, 5648.
(56) Liu, X.; Ide, J. L.; Norton, I.; Marchionni, M. A.; Ebling, M. C.; Wang, L. Y.; Davis, E.; Sauvageot, C. M.; Kesari, S.; Kellersberger, K. A.; Easterling, M. L.; Santagata, S.; Stuart, D. D.; Alberta, J.; Agar, J. N.; Stiles, C. D.; Agar, N. Y. *Sci. Rep.* **2013**, *3*, 2859.
(57) Trim, P. J.; Henson, C. M.; Avery, J. L.; McEwen, A.; Snel, M. F.; Claude, E.; Marshall, P. S.; West, A.; Princivalle, A. P.; Clench, M. R. *Anal. Chem.* **2008**, *80*, 8628.
(58) Prideaux, B.; Dartois, V.; Staab, D.; Weiner, D. M.; Goh, A.; Via, L. E.; Barry, C. E., III; Stoeckli, M. *Anal. Chem.* **2011**, *83*, 2112−2118.
(59) Hamm, G.; Bonnel, D.; Legouffe, R.; Pamelard, F.; Delbos, J. M.; Bouzom, F.; Stauber, J. *J. Proteomics* **2012**, *75*, 4952−4961.
(60) Groseclose, M. R.; Castellino, S. *Anal. Chem.* **2013**, *85*, 10099−10106.
(61) Alexandrov, T. *BMC Bioinf.* **2012**, *13*, S11.
(62) Nimesh, S.; Mohottalage, S.; Vincent, R.; Kumarathasan, P. *Int. J. Mol. Sci.* **2013**, *14*, 11277−11301.
(63) Bemis, K. D.; Harry, A.; Eberlin, L. S.; Ferreira, C.; van de Ven, S. M.; Mallick, P.; Stolowitz, M.; Vitek, O. *Bioinformatics* **2015**, btv146.
(64) Weaver, E. M.; Hummon, A. B.; Keithley, R. B. *Analytical Methods* **2015**.
(65) Benninghoven, A.; Sichtermann, W. K. *Anal. Chem.* **1978**, *50*, 1180−1184.
(66) Fletcher, J. S.; Vickerman, J. C. *Anal. Chem.* **2012**, *85*, 610−639.
(67) Winograd, N. *Anal. Chem.* **2005**, *77*, 142a−149a.
(68) McDonnell, L. A.; Heeren, R. M. A. *Mass Spectrom. Rev.* **2007**, *26*, 606−643.
(69) Sjovall, P.; Greve, T. M.; Clausen, S. K.; Möller, K.; Eirefelt, S.; Johansson, B.; Nielsen, K. T. *Anal. Chem.* **2014**, *86*, 3443−3452.
(70) Anderton, C. R.; Lou, K.; Weber, P. K.; Hutcheon, I. D.; Kraft, M. L. *Biochim. Biophys. Acta* **2011**, *1808*, 307−315.
(71) Lau, K. H.; Christlieb, M.; Schroder, M.; Sheldon, H.; Harris, A. L.; Grovenor, C. R. M. *J. Microsc.* **2010**, *240*, 21−31.
(72) Legin, A. A.; Schintlmeister, A.; Jakupec, M. A.; Galanski, M.; Lichtscheidl, I.; Wagner, M.; Keppler, B. K. *Chem. Sci.* **2014**, *5*, 3135−3143.
(73) Northen, T. R.; Yanes, O.; Northen, M. T.; Marrinucci, D.; Uritboonthai, W.; Apon, J.; Golledge, S. L.; Nordstrom, A.; Siuzdak, G. *Nature* **2007**, *449*, 1033.
(74) Greving, M. P.; Patti, G. J.; Siuzdak, G. *Anal. Chem.* **2011**, *83*, 2−7.
(75) Yanes, O.; Woo, H.-K.; Northen, T. R.; Oppenheimer, S. R.; Shriver, L.; Apon, J.; Estrada, M. N.; Potchoiba, M. J.; Steenwyk, R.; Manchester, M.; Siuzdak, G. *Anal. Chem.* **2009**, *81*, 2969−2975.
(76) O'Brien, P. J.; Lee, M.; Spilker, M. E.; Zhang, C. C.; Yan, Z.; Nichols, T. C.; Li, W.; Johnson, C. H.; Patti, G. J.; Siuzdak, G. *Cancer Metab.* **2013**, *1*, 4.
(77) Venter, A. R.; Douglass, K. A.; Shelley, J. T.; Hasman, G.; Honarvar, E. *Anal. Chem.* **2014**, *86*, 233−249.
(78) Wiseman, J. M.; Ifa, D. R.; Zhu, Y.; Kissinger, C. B.; Manicke, N. E.; Kissinger, P. T.; Cooks, R. G. *Proc. Natl. Acad. Sci. U. S. A.* **2008**, *105* (47), 18120−18125.
(79) Vismeh, R.; Waldon, D. J.; Teffera, Y.; Zhao, Z. *Anal. Chem.* **2012**, *84* (12), 5439−5445.
(80) Kertesz, V.; Van Berkel, G. J.; Vavrek, M.; Koeplinger, K. A.; Schneider, B. B.; Covey, T. R. *Anal. Chem.* **2008**, *80* (13), 5168−5177.
(81) Campbell, D. I.; Ferreira, C. R.; Eberlin, L. S.; Cooks, R. G. *Anal. Bioanal. Chem.* **2012**, *404*, 389−398.
(82) Lanekoff, I.; Heath, B. S.; Liyu, A.; Thomas, M.; Carson, J. P.; Laskin, J. *Anal. Chem.* **2012**, *84*, 8351−8356.
(83) Eikel, D.; Vavrek, M.; Smith, S.; Bason, C.; Yeh, S.; Korfmacher, W. A.; Henion, J. D. *Rapid Commun. Mass Spectrom.* **2011**, *25* (23), 3587−3596.
(84) Swales, J. G.; Tucker, J. W.; Strittmatter, N.; Nilsson, A.; Cobice, D.; Clench, M. R.; Mackay, C. L.; Andren, P. E.; Takáts, Z.; Webborn, P. J.; Goodwin, R. J. *Anal. Chem.* **2014**, *86* (16), 8473−8480.
(85) Parson, W. B.; Koeniger, S. L.; Johnson, R. W.; Erickson, J.; Tian, Y.; Stedman, C.; Schwartz, A.; Tarcsa, E.; Cole, R.; Van Berkel, G. J. *J. Mass Spectrom.* **2012**, *47*, 1420−1428.
(86) Schadt, S.; Kallbach, S.; Almeida, R.; Sandel, J. *Drug Metab. Dispos.* **2012**, *40*, 419−425.
(87) Blatherwick, E. Q.; Van Berkel, G. J.; Pickup, K.; Johansson, M. K.; Beaudoin, M. E.; Cole, R. O.; Day, J. M.; Iverson, S.; Wilson, I. D.; Scrivens, J. H.; Weston, D. J. *Xenobiotica* **2011**, *41*, 720−734.
(88) Nemes, P.; Vertes, A. *Anal. Chem.* **2007**, *79*, 8098−810.
(89) Nemes, P.; Woods, A. S.; Vertes, A. *Anal. Chem.* **2010**, *82*, 982−988.
(90) Shrestha, B.; Nemes, P.; Nazarian, J.; Hathout, Y.; Hoffman, E. P.; Vertes, A. *Analyst* **2010**, *135*, 751−758.
(91) Izmer, A.; Gholap, D.; De Houwer, K.; Cuyckens, F.; Vanhaecke, F. *J. Anal. At. Spectrom.* **2012**, *27*, 413−418.
(92) Madeira, J. M.; Renschler, C. J.; Mueller, B.; Hashioka, S.; Gibson, D. L.; Klegeris, A. *Life Sci.* **2013**, *92*, 1072−1080.
(93) Gholap, D.; Verhulst, J.; Ceelen, W.; Vanhaecke, F. *Anal. Bioanal. Chem.* **2012**, *402*, 2121−2129.
(94) Herdering, C.; Wehe, C. A.; Reifschneider, O.; Raj, I.; Ciarimboli, G.; Diebold, K.; Becker, C.; Sperling, M.; Karst, U. *Rapid Commun. Mass Spectrom.* **2013**, *27*, 2588−2594.
(95) Reifschneider, O.; Wehe, C. A.; Raj, I.; Ehmcke, J.; Ciarimboli, G.; Sperling, M.; Karst, U. *Metallomics* **2013**, *5*, 1440−1447.
(96) Moreno-Gordaliza, E.; Giesen, C.; Lázaro, A.; Esteban-Fernández, D.; Humanes, B.; Cañas, B.; Panne, U.; Tejedor, A.; Jakubowski, N.; Milagros Gómez-Gómez, M. *Anal. Chem.* **2011**, *83*, 7933−7940.
(97) White, E.; Bienemann, A.; Pugh, J.; Castrique, E.; Wyatt, M.; Taylor, H.; Cox, A.; McLeod, C.; Gill, S. *J. Neuro-Oncol.* **2012**, *108*, 77−88.
(98) Bianga, J.; Bouslimani, A.; Bec, N.; Quenet, F.; Mounicou, S.; Szpunar, J.; Bouyssiere, B.; Lobinski, R.; Larroque, C. *Metallomics* **2014**, *6*, 1382−1386.
(99) Breslin, S.; O'Driscoll, L. *Drug Discovery Today* **2013**, *18*, 240−249.
(100) Pampaloni, F.; Reynaud, E.; Stelzer, E. *Nat. Rev. Mol. Cell Biol.* **2007**, *8*, 839−845.
(101) Carletti, E.; Motta, A.; Migliaresi, C. *Methods Mol. Biol.* **2011**, *695*, 17−39.
(102) Haycock, J. W. *Methods Mol. Biol.* **2011**, *695*, 1−15.
(103) Huh, D.; Hamilton, G. A.; Ingber, D. E. *Trends Cell Biol.* **2011**, *21*, 745.
(104) Mehta, G.; Hsiao, A. Y.; Ingram, M.; Luker, G. D.; Takayama, S. *J. Controlled Release* **2012**, *164*, 192−204.
(105) Desoize, B.; Gimonet, D.; Jardiller, J. C. *Anticancer Res.* **1998**, *18*, 4147−4158.
(106) Olive, P. L.; Durand, R. E. *Cancer Metastasis Rev.* **1994**, *13*, 121−138.
(107) Oloumi, A.; MacPhail, S. H.; Johnston, P. J.; Banath, J. P.; Olive, P. L. *Cancer Res.* **2000**, *60*, 5747−5753.
(108) Sutherland, R. M.; Eddy, H. A.; Bareham, B.; Reich, K.; Vanantwerp, D. *Int. J. Radiat. Oncol., Biol., Phys.* **1979**, *5*, 1225−1230.
(109) Durand, R. E.; Sutherland, R. M. *Exp. Cell Res.* **1972**, *71*, 75−80.
(110) Kobayashi, H.; Man, S.; Graham, C. H.; Kapitain, S. J.; Teicher, B. A.; Kerbel, R. S. *Proc. Natl. Acad. Sci. U. S. A.* **1993**, *90*, 3294−3298.
(111) Desoize, B.; Jardillier. *Crit. Rev. Oncol. Hematol.* **2000**, *36*, 193−207.
(112) Friedrich, J.; Seidel, C.; Ebner, R.; Kunz-Schughart, L. A. *Nat. Protoc.* **2009**, *4*, 309−324.
(113) Bryce, N. S.; Zhang, J. Z.; Whan, R. M.; Yamamoto, N.; Hambley, T. W. *Chem. Commun. (Cambridge, U. K.)* **2009**, 2673−2675.
(114) Minchinton, A. I.; Tannock, I. F. *Nat. Rev. Cancer* **2006**, *6*, 583−592.
(115) Kozin, S. V.; Gerweck, L. E. *Br. J. Cancer* **1998**, *77*, 1580−1585.
(116) Pampaloni, F.; Ansari, N.; Stelzer, E. H. *Cell Tissue Res.* **2013**, *352* (1), 161−77.

DOI: 10.1021/acs.analchem.5b00419
Anal. Chem. 2015, 87, 9508−9519

(117) Carver, K.; Ming, X.; Juliano, R. L. *Mol. Ther.–Nucleic Acids* **2014**, *3*, 153.
(118) Hwang, C. W.; Wu, D.; Edelman, E. R. *Circulation* **2001**, *104*, 600−605.
(119) Avery, J. L.; McKewen, A.; Flinders, B.; Francese, S.; Clench, M. *Xenobiotica* **2011**, *41*, 735−742.
(120) Li, H.; Hummon, A. B. *Anal. Chem.* **2011**, *83* (22), 8794−801.
(121) Liu, X.; Weaver, E. M.; Hummon, A. B. *Anal. Chem.* **2013**, *85*, 6295−6302.
(122) Ahlf Wheatcraft, D. R.; Liu, X.; Hummon, A. B. *J. Visualized Exp.* **2014**, *94*, No. e52313.
(123) Taflin, H.; Wettergren, Y.; Odin, E.; Carlsson, G.; Derwinger, K. *Clin. Med. Insights Oncol.* **2014**, *8*, 15−20.
(124) Fazili, Z.; Pfeiffer, C. M. *J. Nutr.* **2012**, *143*, 108−113.
(125) Jägerstad, M.; Jastrebova, J. *Biomed. Chromatogr.* **2014**, *28* (7), 1041−1042.
(126) De Brouwer, V.; Zhang, G. F.; Storozhenko, S.; Van Der Straeten, D.; Lambert, W. E. *Phytochem. Anal.* **2007**, *18* (6), 496−508.
(127) Ahlf, D. R.; Masyuko, R. N.; Hummon, A. B.; Bohn, P. W. *Analyst* **2014**, *139*, 4578−4585.
(128) Niehoff, A. C.; Moosmann, A.; Sobbing, J.; Wiehe, A.; Mulac, D.; Wehe, C. A.; Reifschneider, O.; Blaske, F.; Wagner, S.; Sperling, M.; von Briesen, H.; Langer, K.; Karst, U. *Metallomics* **2014**, *6* (1), 77−81.

DOI: 10.1021/acs.analchem.5b00419
Anal. Chem. 2015, 87, 9508−9519